

# The central engines of two unusual radio-intermediate/quiet active galactic nuclei: III Zw 2 and PG 1407+265

Liang Chen<sup>1</sup>, Xinwu Cao<sup>1</sup> and J. M. Bai<sup>2,3</sup>

## ABSTRACT

We use the accretion disk/corona+jet model to fit the multi-band spectral energy distributions (SEDs) of two unusual radio-intermediate/quiet quasars. It is found that the optical/UV emission of III Zw 2 is probably dominated by the emission from the accretion disk. The X-ray emission should be dominated by the radiation from the jet, while the contribution of the disk corona is negligible. The optical/UV component in the SED of PG 1407+265 can be well modeled as the emission from the accretion disk, while the IR component is attributed to the thermal radiation from the dust torus with an opening angle  $\sim 50^\circ$ . If the X-ray continuum emission is dominated by the synchrotron emission of the jet, the source should be a “high peak frequency blazar”, which obviously deviates the normal blazar sequence. The observed SED can also be fitted quite well by the accretion disk/corona model with the viscosity parameter  $\alpha = 0.5$ . The spectrum of the accretion disk/corona in PG 1407+265 satisfies the weak line quasar criterion suggested in Laor & Davis.

*Subject headings:* galaxies: quasars: individual (III Zw 2 & PG 1407+265) – galaxies: jets – galaxies: active – radiation mechanisms: non-thermal – radiation mechanisms: thermal

---

<sup>1</sup>Key Laboratory for Research in Galaxies and Cosmology, Shanghai Astronomical Observatory, Chinese Academy of Sciences, 80 Nandan Road, Shanghai, 200030, China

<sup>2</sup>National Astronomical Observatories/Yunnan Observatory, Chinese Academy of Sciences, Kunming, 650011, China

<sup>3</sup>Key Laboratory for the Structure and Evolution of Celestial Objects, Chinese Academy of Sciences, Kunming, 650011, China

<sup>†</sup>E-mail: chenliang@shao.ac.cn (LC); cxw@shao.ac.cn (XC); baijinming@ynao.ac.cn (JMB)

## 1. Introduction

In optically selected quasar samples, quasars with similar optical properties exhibit very different properties in radio bands. The radio loudness parameter  $R$ , the ratio of the radio flux at 5 GHz to the optical flux at B-band ( $R \equiv f_{5\text{GHz}}/f_{\text{B}}$ ), is used as an indicator of the radio properties of quasars (Kellermann et al. 1989). Kellermann et al. (1989) found a dichotomy in the radio loudness distribution for an optically selected quasar sample. The quasars with radio loudness  $R > 10$  are defined as radio-loud (RL) quasars, while those with  $R \leq 10$  are named as radio-quiet (RQ) quasars. It was found that RL active galactic nuclei (AGNs) have powerful relativistic jets, while most of RQ AGNs have no or very weak jets. The distribution of radio-loudness may provide useful clues on the jet formation mechanism of AGNs and the disk-jet connection, which was explored by many previous authors (e.g., White et al. 2000; Ivezić et al. 2002; Ho & Peng 2001; Cirasuolo et al. 2003; Merloni et al. 2003; Falcke et al. 2004; Liu et al. 2006; Sikora et al. 2007; Broderick & Fender 2011). The FIRST (Faint Images of the Radio Sky at Twenty Centimeters) detected quasars showed that the radio loudness distribution is not bimodal, but rather continuous (White et al. 2000). It is still debating on whether the radio-loudness distribution is bimodal or continuous (see, Ivezić et al. 2002; Cirasuolo et al. 2003).

The radio-loudness parameter can be a good indicator of the jet properties of AGNs in the sense of statistics. Miller et al. (1993) and Falcke et al. (1996) identified a number of quasars with “radio intermediate loudness”. They suggested that these sources might be relativistically boosted radio-weak quasars (“radio-weak blazars”). In fact, the very long baseline interferometry (VLBI) observations have revealed that many RQ/radio-intermediate AGNs exhibit jet structure and high-brightness temperature radio cores (e.g., Kukula et al. 1998; Blundell & Beasley 1998; Blundell et al. 2003; Ulvestad et al. 2005; Wang et al. 2006; Leipski et al. 2006). In this work, we choose two unusual RQ/radio intermediate sources with relativistic jets, III Zw 2 and PG 1407+265, to explore the physics of the disk-jet connection in this kind of the sources. As these two sources have both RL and RQ characteristics, the present investigation may reveal the relation of the disk-jet connection with the radio-loudness parameter, which may provide clues on the origin of the radio-loudness distribution.

Arp (1968) classified III Zw 2 (PG 0007+106, Mrk 1501,  $z = 0.089$ ) as a Seyfert I galaxy, which is also included in the PG quasar sample (Schmidt & Green 1983). It is hosted in a spiral galaxy (Hutchings & Campbell 1983), which is typical characteristics of RQ AGNs. The extended radio emission is very weak compared with its core emission ( $\sim 50 - 100$  mJy at 1.4 GHz, Unger et al. 1987; Brunthaler et al. 2005), and superluminal motions of the jet components in this source have been detected in the VLBA (Very Long Baseline Array) images (Brunthaler et al. 2000). The apparent velocity of the moving jet components is

$\beta_{\text{app}} = 1.25 \pm 0.09$  in units of light speed is derived from the VLBA images at 43 GHz. III Zw 2 exhibits violent variability throughout all wavebands (for example, more than an order of magnitude of variability in radio bands, see Salvi et al. 2002). Chen et al. (2010) modeled the multi-waveband SED of this sources, and suggested that III Zw 2 is a possible  $\gamma$ -ray source and could be detected by the *Fermi*/LAT in the future. This source possesses typical blazar-like properties, however, it is included in the radio-intermediate sample (Falcke et al. 1996).

PG 1407+265 is a RQ AGN ( $z = 0.94$ , Kellermann et al. 1989; McDowell et al. 1995) with some unusual properties. Its flux ratios in the radio, X-ray, and optical wavebands are typical of normal RQ quasars (Plotkin et al. 2010). McDowell et al. (1995) found that the emission lines of PG 1407+265 have very small equivalent widths (except for  $H\alpha$ ), but the full width at half-maximum (FWHM) reaches  $v \approx 7000 - 12000 \text{ km s}^{-1}$ . This is a weak line quasar (WLQ). The nature of WLQs is still unclear so far, though they are extensively studied (see, Laor & Davis 2011, and the references therein). The optical-to-X-ray spectral index,  $\alpha_{\text{ox}}$ , of typical RQ AGNs ranges from 1.2 to 1.8, and the slope steepens with increasing UV luminosity (Strateva et al. 2005). During the high state of PG 1407+265, the optical-to-X-ray spectrum is flat ( $\alpha_{\text{ox}}=1.09$ ), and there are larger fluctuations in the X-ray bands than the UV bands (i.e., the slope flattens with increasing luminosity, Gallo 2006), which seems to be different from that in typical RQ AGNs. It is found that the UV variability correlates with that of the X-ray emission in the high state, and Gallo (2006) suggested that the soft X-rays may be the jet’s non-thermal emission in the high state. This implies that both the emission in the optical and X-ray bands may come from the jets. It is interesting to note that the source PG 1407+265 may probably have a relativistic jet moving toward us with a Doppler factor of  $\delta \gtrsim 10$  from its radio morphology and the variations in radio wavebands (Blundell et al. 2003). To our knowledge, PG 1407+265 is the only RQ AGN with relativistic jets reported in the literature so far. Chen & Bai (2011) fitted the multi-waveband SED of this source with the homogeneous sphere jet model, and they found that the jet is required to be in very extreme conditions. Thus, they suggested that the radiation of the accretion disk may not be negligible in the optical/UV bands of the SED for this source.

In this paper, we adopt an accretion disk/corona+jet model to explore the disk-jet connection in these two unusual AGNs. In Section 2, we give a brief summary of the jet and the disk-corona emission models used to fit the observed SEDs. Section 3 contains the results. The discussion and conclusions are given in Sections 4 and 5. Throughout this paper, a cosmology with  $H_0 = 70 \text{ km s}^{-1}\text{Mpc}^{-1}$ ,  $\Omega_{\text{m}} = 0.3$  and  $\Omega_{\Lambda} = 0.7$  is adopted.

## 2. The model

The homogeneous sphere jet model was widely used to explain the observed SEDs of blazars, with which the main features of the blazars’ spectra can be well reproduced (e.g., Tavecchio et al. 1998, 2001; Celotti & Ghisellini 2008). For RQ AGNs, the accretion disk/corona model was developed to explain the optical/UV and X-ray spectra (e.g., Haardt & Maraschi 1991, 1993). In this work, we adopt the homogeneous sphere jet+accretion disk/corona model to fit the observed SEDs of these two AGNs, and their physical properties can be derived. We briefly describe the jet, and the accretion disk/corona models employed in this work as follows.

### 2.1. Jet model

In this paper, we use one zone synchrotron+inverse Comptonization (IC) models to calculate the jet emission of III Zw 2 and PG 1407+265. The model was widely used in blazar SED modeling (e.g., Ghisellini et al. 2010, and the references therein). The emission region is assumed to be a homogeneous sphere with radius  $R$  embedded in the magnetic field  $B$  (see, Tavecchio et al. 1998, 2001; Celotti & Ghisellini 2008; Ghisellini et al. 2010, for the details). A broken power law electron energy distribution,

$$N(\gamma) = \begin{cases} N_0 \gamma^{-p_1} & \gamma_{\min} \leq \gamma \leq \gamma_0 \\ N_0 \gamma_0^{p_2-p_1} \gamma^{-p_2} & \gamma_0 < \gamma \leq \gamma_{\max}, \end{cases} \quad (1)$$

is assumed in our calculations. Such a broken power law distribution could be the result of the balance between the particle cooling and escape rates in the blob (see, Kardashev 1962; Sikora et al. 1994; Inoue & Takahara 1996; Kirk et al. 1998; Ghisellini et al. 1998, for the detailed discussion). The parameters of this model include, the radius  $R$  of the blob, the magnetic field strength  $B$ , electron break energy  $\gamma_0$ , the minimum and maximum energy  $\gamma_{\min}$ ,  $\gamma_{\max}$ , of the electrons, the normalization of the particle number density  $N_0$ , and the indexes  $p_{1,2}$  of the broken power law particle distribution. The observed spectrum of the jet can be calculated when the Lorentz factor  $\Gamma = 1/\sqrt{1-\beta^2}$ , the viewing angle  $\theta$  of the jet with respect with the line of sight, and the spectrum of the external seed photons, are supplied. The frequency and luminosity can be transformed from the jet frame to observational frame as:  $\nu = \delta \nu'/(1+z)$  and  $\nu L_\nu = \delta^4 \nu' L'_{\nu'}$ , where the Doppler factor  $\delta = 1/[\Gamma(1-\beta \cos \theta)]$ , and the prime represents the value measured in the jet frame. The synchrotron self-absorption and the Klein-Nishina effect in the inverse Compton scattering are properly considered in our calculations (see, Rybicki & Lightman 1979; Blumenthal & Gould 1970). Both the self-synchrotron Compton (SSC) scattering and external Compton (EC) scattering are included in the calculation of the Compton scattering in the blob.

In this homogeneous sphere model, the jet power can be calculated if all the physical quantities of the sphere are specified,

$$L_{\text{jet}} \simeq \pi R^2 \beta \Gamma^2 c U'_{\text{tot}}, \quad (2)$$

where the total energy density measured in the rest frame of the blob,

$$U'_{\text{tot}} = U'_e + U'_B + U'_p.$$

The energy density for electrons  $U'_e = m_e c^2 \int N(\gamma) \gamma d\gamma$ , while the proton energy density  $U'_p = U'_e (m_p/m_e) / \langle \gamma \rangle$  if charge neutrality for pure hydrogen plasma is assumed (Celotti & Fabian 1993; Celotti & Ghisellini 2008). The broad waveband SED from high frequency radio emission to  $\gamma$ -ray bands can be modeled with this homogeneous sphere model (e.g., Celotti & Ghisellini 2008; Ghisellini et al. 2010). The emission from blazars in low frequency radio band may dominantly be radiated from the inner conical jet near the black hole (e.g., Blandford & Konigl 1979; Konigl 1981; Ghisellini et al. 1985; Jiang et al. 1998), which is beyond the scope of this work. In this work, we use the conventional homogeneous sphere model to fit the observed SEDs from high frequency radio emission to  $\gamma$ -ray bands, which is similar to most of the previous works (e.g., Celotti & Ghisellini 2008; Ghisellini et al. 2010).

## 2.2. Accretion disk/corona model

The observed UV/optical continuum emission of AGNs is thought to be the thermal emission from the standard geometrically thin, optically thick accretion disks (e.g., Shields 1978; Malkan & Sargent 1982; Sun & Malkan 1989), while the observed power-law hard X-ray spectra of RQ AGNs are most likely due to the inverse-Compton scattering of soft photons on a population of hot electrons in the corona above the disk (Galeev et al. 1979; Haardt & Maraschi 1991, 1993). In the accretion disk-corona model, such soft photons are from the cold disk, a fraction of which are Compton scattered by the hot electrons in the corona above the cold disk to the hard X-ray energy band. The disk-corona model was extensively explored in many previous works (e.g., Haardt & Maraschi 1991, 1993; Svensson & Zdziarski 1994; Kawaguchi et al. 2001; Liu et al. 2002; Cao 2009). In this disk-corona scenario, most of the gravitational energy of the accreting matter is released in the cold disk, and a fraction of which is transported into the corona probably by magnetic fields. The magnetic fields generated in the cold disk are strongly buoyant, and a substantial fraction of magnetic energy is transported vertically to heat the corona above the disk with the reconnection of the fields (e.g., Di Matteo 1998; Di Matteo et al. 1999; Merloni & Fabian 2001, 2002; Cao 2009). In this work, we adopt the model given in Cao (2009) to calculate

the spectrum of the accretion disk/corona system. We summarize the accretion disk-corona model in this sub-section.

The gravitational power dissipated in unit surface area of the accretion disk is given by

$$Q_{\text{dissi}}^+ = \frac{3}{8\pi} \dot{M} \Omega_{\text{k}}(R)^2 \left[ 1 - \left( \frac{R_{\text{in}}}{R} \right)^{1/2} \right], \quad (3)$$

where  $\dot{M}$  is the mass accretion rate of the disk,  $\Omega_{\text{k}}(R)$  is the Keplerian velocity at radius  $R$ , and  $R_{\text{in}} = 3R_{\text{S}}$  (Shakura & Sunyaev 1973). The Schwarzschild radius  $R_{\text{S}} = 2GM_{\bullet}/c^2$ , where  $M_{\bullet}$  is the black hole mass. The accretion disk luminosity is

$$L_{\text{disk}} = 4\pi \int Q_{\text{dissi}}^+ R dR = \frac{GM_{\bullet} \dot{M}}{2R_{\text{in}}}. \quad (4)$$

In the absence of the corona, the surface temperature  $T_{\text{s}}$  of the disk as a function of radius  $R$  can be calculated with  $\sigma T_{\text{s}}^4 = Q_{\text{dissi}}^+$ , and the spectrum of the disk is available by integrating blackbody emissivity  $B_{\nu}(R)$  over radius  $R$  (Shakura & Sunyaev 1973). In this case, the spectrum of the accretion disk can be derived when the black hole mass and the accretion rate are specified.

In the accretion disk/corona system, the corona is assumed to be heated by the reconnection of the magnetic fields generated by the buoyancy instability in the disk. The power dissipated in the corona is estimated with,

$$Q_{\text{cor}}^+ = p_{\text{m}} v_{\text{p}} = \frac{B^2}{8\pi} v_{\text{p}}, \quad (5)$$

where  $p_{\text{m}}$  is the magnetic pressure in the disk, and  $v_{\text{p}}$  is the velocity of the magnetic flux transported vertically in the disk (Di Matteo 1998). The rising speed  $v_{\text{p}}$  is assumed to be proportional to the internal Alfvén velocity, i.e.,  $v_{\text{p}} = b v_{\text{A}}$ , in which  $b$  is of the order of unity for extremely evacuated magnetic tubes. We adopt  $b = 1$  in all our calculations of this work.

The soft photons from the disk are Compton scattered by the hot electrons in the corona to X-ray bands, and about half of the scattered photons are intercepted by the disk. The reflection albedo  $a$  is relatively low,  $a \sim 0.1 - 0.2$ , and most of the incident photons from the corona are re-radiated as blackbody radiation (e.g., Zdziarski et al. 1999). Thus, the energy equation for the cold disk is

$$Q_{\text{dissi}}^+ - Q_{\text{cor}}^+ + \frac{1}{2}(1 - a)Q_{\text{cor}}^+ = \frac{4\sigma T_{\text{disk}}^4}{3\tau}, \quad (6)$$

where  $T_{\text{disk}}$  is the effective temperature in the mid-plane of the disk, and  $\tau = \tau_{\text{es}} + \tau_{\text{ff}}$  is the optical depth in vertical direction of the disk. In this work, we adopt  $a = 0.15$  in all our calculations.

The detailed physics for generating magnetic fields in the accretion disk is still quite unclear, and there are three different magnetic stress tensors were usually adopted,

$$\tau_{r\varphi} = p_m = \begin{cases} \alpha p_{\text{tot}} \\ \alpha p_{\text{gas}} \\ \alpha \sqrt{p_{\text{gas}} p_{\text{tot}}}, \end{cases} \quad (7)$$

where  $\alpha$  is the viscosity parameter (see Shakura & Sunyaev 1973; Sakimoto & Coroniti 1981; Taam & Lin 1984). The parameters of the disk-corona model include the black hole mass  $M_\bullet$ , the dimensionless mass accretion rate  $\dot{m}$  ( $\dot{m} = \dot{M}/\dot{M}_{\text{Edd}}$ ,  $\dot{M}_{\text{Edd}} \equiv L_{\text{Edd}}/\eta_{\text{rad}}c^2$ , and the conventional radiative efficiency  $\eta_{\text{rad}} = 0.1$  is adopted), and the viscosity parameter  $\alpha$  (see Cao 2009, for the details).

### 3. Results

We search the literature for the observational data of the multi-waveband SEDs of these two sources from radio to X-ray bands (Salvi et al. 2002; Kaastra & de Korte 1988, and *NED*<sup>1</sup>). Obviously, simultaneous broad band SEDs are desired to be used to model the disk-jet systems in these sources. For III Zw 2, we search the literature and collect a broad band SED, which is quasi-simultaneous within half a year (see Table 2). This source shows long-term variability on time scale of a few years, which is longer than the temporal span of the quasi-simultaneous data. Therefore, we mainly adopt this SED for our model fitting. For the source PG 1407+265, we collect and list all X-ray observations in Table 4. We note that the GINGA observation (Jun. 1987) is roughly simultaneous with IR and optical observations (see Table 3 and 4). Unfortunately, only 2-10 keV flux is available without spectral index. It can be seen that the 2-10 keV flux of observation on Jan. 17, 1981 by EINSTEIN is similar to that of GINGA observation. We therefore use EINSTEIN observation data in the quasi-simultaneous spectrum of this source (see Table 4).

#### 3.1. III Zw 2

We search the literature and collect the quasi-simultaneous SED of III Zw 2 from radio to X-ray bands, which is plotted in Figure 1 (the data are listed in Table 2). Salvi et al. (2002) estimated the central black hole mass  $M_\bullet = 10^9 M_\odot$  from the width of the broad-line H $\beta$  of this source. Superluminal motion of the jet component with apparent velocity

---

<sup>1</sup><http://ned.ipac.caltech.edu/>

$\beta_{\text{app}} = 1.25 \pm 0.09$  in III Zw 2 has been detected with VLBA observations (Brunthaler et al. 2000). Popović et al. (2003) derived the inclination angle of the emission line disk  $\theta = 12^\circ \pm 5^\circ$  for III Zw 2 from its broad emission line profile. Assuming the jet to be perpendicular to the emission line disk, the Lorentz factor of the jet,  $\Gamma \simeq 2.06$ , and the Doppler factor,  $\delta \simeq 3.35$ , are derived.

In the calculations of the spectra from the jets, we have considered both the SSC and EC mechanisms. The external soft seed photons from the broad line region (BLR) are considered in our calculations. The VLBA observations and the variability in radio bands imply that the location of the blob is within the BLR (see Brunthaler et al. 2000). The radius of the emission region is estimated with the minimum variability time scale  $R \approx ct_{\text{var}}\delta/(1+z) \approx 1.5 \times 10^{16}$  cm (Jang & Miller 1997). Kaastra & de Korte (1988) estimated the size of the BLR  $\approx 10^{18}$  cm, and the photon energy density within the BLR  $U_{\text{ext}} \approx 3.8 \times 10^{-4}$  erg cm $^{-3}$ . Thus, the multi-waveband spectrum of the jet can be calculated if the values of the parameters,  $N_0$ ,  $B$ ,  $\gamma_0$ ,  $\gamma_{\text{min}}$ ,  $p_1$  and  $p_2$ , are provided. Besides the spectrum of the jet, we need to calculate the spectra from the accretion disk/corona system in this source. First, we consider the simplest case, i.e., a bare accretion disk without a corona. In this case, the spectrum of the accretion disk is only dependent on the mass accretion rate (see Section 2).

From Figure 1, it can be seen that the quasi-simultaneous SED seems to show two bumps at IR and UV bands respectively. The UV bump is a typical character of RQ AGN, which can be explained as the thermal emission from an accretion disk emission. We model the UV bump as disk emission, and jet emission accounts for the IR bump. In the model fitting the quasi-simultaneous SED, the least squares method is adopted to derive the best fitted model parameters. The model parameters, the accretion rate  $\dot{m}$ , the minimum electron energy  $\gamma_{\text{min}}$ , and the magnetic field strength  $B$ , are carefully tuned in order to obtain the best model fitting to the quasi-simultaneous SED. The best fitting parameters are listed in Table 1 (see Figure 1). With the values of the parameters determined from the fitting of the SEDs, the jet power can be calculated with Equation (2). In this case, jet power is  $L_{\text{jet}}^{\text{sim}} \approx 1.5 \times 10^{45}$  erg s $^{-1}$  and the accretion disk luminosity  $L_{\text{disk}}^{\text{sim}} \approx 1.1 \times 10^{45}$  erg s $^{-1}$ .

We also repeat our calculations by adopting the accretion disk/corona model instead of the bare accretion disk model as described above. There are different choices of magnetic stresses (see Equation 7). Our results show that the contribution to the X-ray continuum spectra in this source is always negligible (see Table 1).

We plot the sensitivity of the detector of *Fermi*/LAT in the Figure 1 (purple lines, McEnery et al. 2004). It can be seen that if the optical/UV emission is dominantly from the accretion disk, the predicted  $\gamma$ -ray flux is below the sensitivity of *Fermi*/LAT.



### 3.2. PG 1407+265

The quasi-simultaneous SED of PG 1407+265 shows clear evidence of an optical-UV bump (see Figure 2). Hryniewicz et al. (2010) estimated the black hole mass of this source to be  $6 \times 10^9 M_\odot$ . There are no (quasi-)simultaneous optical/IR spectra corresponding to the high state in the X-ray band. Thus, we have to limit our model fittings to the quasi-simultaneous SED in the low state. Blundell et al. (2003) suggested that there is a relativistic jet in PG 1407+265, and the Doppler factor of the jet is estimated as  $\delta \gtrsim 10$ . We adopt  $\delta = 10$  in our calculations for this source. The procedure of fitting its SED is the same as that for III Zw 2. We find that the optical/UV component in the SED may probably be from the accretion disk, while the origin of the IR component is still uncertain. There are two possibilities: the synchrotron emission from the jet, or the thermal radiation from the dust torus irradiated by the radiation of the central engine. In the case of the synchrotron emission, the minimum electron energy can be constrained,  $\gamma_{\min} \approx 13.5$ , if equipartition between magnetic field and electron+proton energy is assumed. The jet power is  $L_{\text{jet}} \approx 1.1 \times 10^{46} \text{ erg s}^{-1}$ , while the disk luminosity is  $L_{\text{disk}} \approx 6.8 \times 10^{46} \text{ erg s}^{-1}$ . If the IR component is from the dust torus, our calculations require the minimum electron energy  $\gamma_{\min} \approx 4.6$ , and the jet power is  $L_{\text{jet}} \approx 3.3 \times 10^{44} \text{ erg s}^{-1}$ , which is significantly lower than the disk luminosity. All the model parameters adopted for different cases are listed in Table 5.

In order to explore the origin of the X-ray emission in PG 1407+265, we also model the SED of this source by including the contribution of the corona above the disk. In our calculations, we adopt different magnetic stresses respectively, and find that the contribution of the corona to the X-ray spectrum is always negligible, unless the stress  $\tau_{r\phi} = p_m = \alpha p_{\text{tot}}$  is adopted with an relatively high viscosity parameter:  $\alpha \sim 0.5$  (see Figure 3).

### 3.3. Blazar sequence

We compare these two sources with the well studied blazar sample (Celotti & Ghisellini 2008). In Figure 4, the blazar sequence is plotted, and we find that these two sources roughly follow the correlation defined by the blazar sample, except the source PG 1407+265 if the IR component is from the dust torus and the X-ray emission is the synchrotron emission from the jet. We also compare the relation of jet power and disk luminosity with that of the blazar sample in Figure 5, in which the blazar sample is taken from Ghisellini et al. (2010).

#### 4. Discussion

The simultaneous SEDs either in the high or low states are not available for III Zw 2, and only a quasi-simultaneous SED is obtained by searching the data in literature. This quasi-simultaneous SED shows a big blue bump, which is a typical character of RQ quasar and can be modeled quite well by the accretion disk model (see Figure 1). Compared with RQ AGNs, it is known that relatively high polarization in the optical waveband is observed in blazars, because the emission in this waveband is dominated by the synchrotron emission from the relativistic jets. We note that almost no polarization has been observed in the optical waveband for III Zw 2 ( $\sim 0.28 \pm 0.19\%$ , Berriman et al. 1990), and the amplitude of its optical variability is smaller than the radio and X-ray emission (Salvi et al. 2002), which imply that the optical/UV emission in this source may not be dominantly from the jet. We estimate the thermal timescale of the accretion disk (assuming black hole spin  $a = 0$ , and using the same method as that in Liu et al. 2008),  $\tau_{\text{thermal}} \approx 2 - 5$  yr for this source in the low or the high states. This is roughly consistent with the observed optical/UV variability timescales (Salvi et al. 2002). Chen et al. (2010) showed that the predicted  $\gamma$ -ray emission can be detected by *Fermi*/LAT, if the jet emission is responsible for the optical/UV continuum emission. However, the model fittings to the simultaneous SED of this source in this work show that the UV/optical emission originates from the accretion disk (see Figure 1), and the  $\gamma$ -ray emission from the jet is below the sensitivity of *Fermi*/LAT. We note that III Zw 2 is not included in either 1LAC (the first LAT AGN Catalog, Abdo et al. 2010) or 2LAC (the second LAT AGN Catalog, Ackermann et al. 2011). We suggest that the optical/UV continuum spectra of this source may probably be dominantly emitted from the accretion disk. This issue can be sorted out if the simultaneous multi-waveband observations on this source both in low and high states are performed in the future.

We also calculate the X-ray spectrum of the corona above the disk, and find that the contribution of the corona to the X-ray emission is always negligible, i.e., the X-ray continuum spectra are mainly emitted from the relativistic jet in this source. Sikora et al. (2007) investigated the radio loudness of a sample with 199 sources consisting of broad-line radio galaxies (BLRGs), radio-loud quasars (RLQs), Seyfert galaxies (SGs), low-ionization nuclear emission-line region galaxies (LINERs), and Fanaroff-Riley type I radio galaxies (FR I RGs). They found that there are two distinct, approximately parallel tracks in the plot of  $\log R - \log \lambda$  (the Eddington ratio  $\lambda \equiv L_{\text{bol}}/L_{\text{Edd}}$ , where  $L_{\text{bol}}$  is the bolometric luminosity and  $L_{\text{Edd}}$  is the Eddington luminosity). We compare III Zw 2 with the results in Sikora et al. (2007), and find that this source locates between the RL and RQ tracks (Eddington ratio:  $\lambda^{\text{low}} \approx 0.019$ ,  $\lambda^{\text{high}} \approx 0.072$ ,  $\lambda^{\text{sim}} \approx 0.039$ ; radio-loudness  $R \sim 100 - 200$ , Falcke et al. (1996); Brunthaler et al. (2000)).

Strong Fe  $K\alpha$  line emission with equivalent width  $EW \simeq 220 \text{ \AA}$  has been detected in III Zw 2 (Jiménez-Bailón et al. 2005). It roughly follows the relation between the equivalent width and luminosity for RQ quasars, of which the X-ray continuum emission is supposed to be from the accretion disk/corona system (Nandra et al. 1997). Our results suggest that only a small fraction of the observed X-ray continuum is from the corona of the accretion disk, which implies that this source in fact deviates significantly from the relation between the equivalent width and luminosity defined by the RQ quasar sample if the X-ray continuum emission from the jet is properly subtracted in this source. The X-ray emission from the corona is obviously not enough to power such a strong Fe  $K\alpha$  in this source, and therefore the detailed studies on X-ray reflection geometry in III Zw 2 may be necessary for resolving this issue, which is beyond the scope of this work.

The SED of PG 1407+265 exhibits a clear component in optical/UV bands, which can be well fitted by the accretion disk model (see, Figure 2). Chen & Bai (2011) fitted the multi-band SED of this source using the one-zone jet model, and found that extreme values of some model parameters are required. Similar to III Zw 2, almost no polarization in optical emission has been detected in this source ( $\sim 0.24 \pm 0.16\%$ , Berriman et al. 1990), which may also suggest that most of the optical-UV emission may not come from the jet.

The origin of the X-ray emission in this source is somewhat uncertain, which could be dominantly either from the jet or the corona above the disk. We firstly adopt the jet+accretion disk/corona model to fit its SEDs. In this case, our results show that the X-ray emission is dominantly from the jet. Unlike III Zw 2, a component in IR wave bands has been observed in PG 1407+265, which may originate from the synchrotron emission from the jet, or the thermal radiation from the dust torus irradiated by the radiation of the central engine. In the case of the synchrotron emission, the derived jet power is  $L_{\text{jet}} \approx 1.1 \times 10^{46} \text{ erg s}^{-1}$ , which is lower than the disk luminosity ( $L_{\text{disk}} \approx 6.8 \times 10^{46} \text{ erg s}^{-1}$ ). If the IR component is alternatively assumed to be emitted from the dust torus, our calculations indicate that the jet power  $L_{\text{jet}} \approx 3.3 \times 10^{44} \text{ erg s}^{-1}$ , which is also significantly lower than the disk luminosity. Blundell et al. (2003) estimated the lower limit on the jet power in this source,  $\sim 7 \times 10^{43} \text{ erg s}^{-1}$ , by assuming minimum of the total energy density, in which the minimum magnetic field strength  $B_{\text{min}}$  is adopted. Considering that the realistic field strength could be significantly higher than  $B_{\text{min}}$ , their estimate of the lower limit on jet power is consistent with our results in the case of the IR emission being from the torus. The opening angle of the dust torus can be estimated from the ratio of IR to optical/UV fluxes by assuming that the radiation of the disk is absorbed by the dust torus and re-radiates in IR wavebands (see Cao 2005, for the detailed discussion). The ratio of IR to optical/UV emission  $\sim 0.6$  for PG 1407+265, and the torus opening angle  $\sim 50^\circ$  is inferred, which is typical for RQ AGNs (Elvis et al. 1994; Cao 2005; Shang et al. 2011). We find that the X-ray emission is

dominated by the synchrotron emissions from the jet (see the lower panel of Figure 2), and this source should be a “high peak frequency blazar”. This source is luminous, and it is quite different compared with normal blazars, because the blazar sequence expects a high peak frequency blazar when its luminosity is low (Fossati et al. 1998; Ghisellini et al. 1998; Chen & Bai 2011).

In order to investigate the origin of the X-ray emission in this source, we alternatively adopt the accretion disk/corona model to fit the SED for this source. We find that the spectra in the optical/UV and X-ray bands can be fairly well fitted with the magnetic stress  $\tau_{\text{r}\phi} = \alpha p_{\text{tot}}$ , provided  $\dot{m} = 0.3$  and  $\alpha = 0.5$  are adopted (see Figure 3). However, we note that the variability of the X-ray emission in this source can be around an order of magnitude between its low and high states (see Figure 3), which is more violent than normal RQ quasars. Future simultaneous multi-band (UV/optical+X-ray) observations on this source will help resolve this issue. In the accretion disk/corona model, the variability in the X-ray band may lead to variable optical-UV emission, and vice versa. The observational data show strong variability in the X-ray band of this source, while no evidence of similar variability is found in the optical/UV band. Further simultaneous multi-waveband observations is expected to attack the nature of the X-ray emission in this source. We compare PG 1407+265 with the results in Sikora et al. (2007), and find that this source locates in the RQ track (Eddington radio  $\lambda \approx 0.33$ ; radio-loudness  $R \approx 0.44, 3.43$ , Wilkes & Elvis (1987); Kellermann et al. (1989)). Therefore, PG 1407+265 could be a typical RQ quasar, but contains relativistic weak jets.

The nature of WLQs is still unclear. Laor & Davis (2011) proposed that the accretion disk temperature decreases with increasing black hole mass, and the fraction of the photons with the energy that can ionize the BLR decreases. This may account for the weak line emission in some AGNs. They suggested that, the quasar will be lineless if the fraction of the accretion disk emission above the frequency  $\nu = 3.29 \times 10^{15}$  Hz is less than 0.01 ( $L_{\nu > 3.29 \times 10^{15} \text{ Hz}}/L \lesssim 0.01$ ), while a weak line quasar appears if  $L_{\nu > 3.29 \times 10^{15} \text{ Hz}}/L \lesssim 0.1$ . PG 1407+265 is the first WLQ studied in detail (McDowell et al. 1995). We calculate the fraction of disk-corona emission above the frequency,  $L_{\nu > 3.29 \times 10^{15} \text{ Hz}}/L \approx 0.08 - 0.1$ , which satisfies the WLQ criterion suggested by Laor & Davis (2011).

We compare these two sources with the well studied blazar sample Celotti & Ghisellini (2008). We find that these two sources roughly follow the blazar sequence defined by the blazar sample, and also compare the relation of jet power and disk luminosity with that of blazars. We find that these two sources do not deviate much from the blazars, except the source PG 1407+265, if its IR component is assumed to be from the dust torus and the X-ray emission is the synchrotron emission from the jet.

## 5. Summary

We summarize the main conclusions of this paper as follows.

1. The optical/UV emission of III Zw 2 is dominantly from the accretion disk. The X-ray emission should be dominated by the radiation from the jet, while the contribution of the disk corona is negligible.
2. The predicted  $\gamma$ -ray emission is below the sensitivity of *Fermi*/LAT, provided the UV is emission originated from the accretion disk.
3. The optical/UV component in the SED of PG 1407+265 can be well modeled as the emission from the accretion disk, while the IR component is attributed to the thermal radiation from the dust torus with an opening angle  $\sim 50^\circ$ . If the X-ray continuum emission is dominantly from the jet, the source should be a “high peak frequency blazar”, which obviously deviates the normal blazar sequence.
4. The observed SED can also be fitted quite well by the accretion disk/corona model with the viscosity parameter  $\alpha = 0.5$ . The spectrum of the accretion disk/corona in the WLQ PG 1407+265 satisfies the WLQ criterion suggested by Laor & Davis (2011).

We thank the anonymous referee for insightful comments and constructive suggestions. This work is supported by the NSFC (grants 10821302, 10833002, 11173043, 11133006, 10973034, 10903025, 11078008, and 11103060), the National Basic Research Program of China (grant 2009CB824800), the Science and Technology Commission of Shanghai Municipality (10XD1405000), and the CAS/SAFEA International Partnership Program for Creative Research Teams (KJCX2-YW-T23).

## REFERENCES

- Abdo, A. A., Ackermann, M., Ajello, M., et al. 2010, *ApJ*, 715, 429
- Ackermann, M., Ajello, M., Allafort, A., et al. 2011, *ApJ*, 743, 171
- Arp, H. 1968, *ApJ*, 152, 1101
- Barvainis, R., Lonsdale, C., & Antonucci, R. 1996, *AJ*, 111, 1431
- Berriman, G., Schmidt, G. D., West, S. C., & Stockman, H. S. 1990, *ApJS*, 74, 869
- Blandford, R. D., & Konigl, A. 1979, *ApJ*, 232, 34
- Blumenthal, G. R., & Gould, R. J. 1970, *Reviews of Modern Physics*, 42, 237
- Blundell, K. M., & Beasley, A. J. 1998, *MNRAS*, 299, 165
- Blundell, K. M., Beasley, A. J., & Bicknell, G. V. 2003, *ApJ*, 591, L103
- Broderick, J. W., & Fender, R. P. 2011, *MNRAS*, 417, 184
- Brunthaler, A., Falcke, H., Bower, G. C., et al. 2005, *A&A*, 435, 497
- Brunthaler, A., Falcke, H., Bower, G. C., et al. 2000, *A&A*, 357, L45
- Cao, X. 2009, *MNRAS*, 394, 207
- Cao, X. 2005, *ApJ*, 619, 86
- Celotti, A., & Fabian, A. C. 1993, *MNRAS*, 264, 228
- Celotti, A., & Ghisellini, G. 2008, *MNRAS*, 385, 283
- Chen, L., & Bai, J. M. 2011, *ApJ*, 735, 108
- Chen, L., Bai, J.-M., Zhang, J., & Liu, H.-T. 2010, *Research in Astronomy and Astrophysics*, 10, 707
- Chen, L., & Bai, J. 2011, *Science in China G: Physics and Astronomy*, 54, 183
- Cirasuolo, M., Celotti, A., Magliocchetti, M., & Danese, L. 2003, *MNRAS*, 346, 447
- Di Matteo, T. 1998, *MNRAS*, 299, L15
- Di Matteo, T., Celotti, A., & Fabian, A. C. 1999, *MNRAS*, 304, 809

- Elvis, M., Wilkes, B. J., McDowell, J. C., et al. 1994, *ApJS*, 95, 1
- Falcke, H., K rding, E., & Markoff, S. 2004, *A&A*, 414, 895
- Falcke, H., Sherwood, W., & Patnaik, A. R. 1996, *ApJ*, 471, 106
- Fang, T., Canizares, C. R., & Marshall, H. L. 2005, *ApJ*, 633, 61
- Fossati, G., Maraschi, L., Celotti, A., Comastri, A., & Ghisellini, G. 1998, *MNRAS*, 299, 433
- Galeev, A. A., Rosner, R., & Vaiana, G. S. 1979, *ApJ*, 229, 318
- Gallo, L. C. 2006, *MNRAS*, 365, 960
- George, I. M., Turner, T. J., Yaqoob, T., et al. 2000, *ApJ*, 531, 52
- Ghisellini, G., Celotti, A., Fossati, G., Maraschi, L., & Comastri, A. 1998, *MNRAS*, 301, 451
- Ghisellini, G., Maraschi, L., & Treves, A. 1985, *A&A*, 146, 204
- Ghisellini, G., Tavecchio, F., Foschini, L., et al. 2010, *MNRAS*, 402, 497
- Haardt, F., & Maraschi, L. 1991, *ApJ*, 380, L51
- Haardt, F., & Maraschi, L. 1993, *ApJ*, 413, 507
- Haas, M., Klaas, U., M ller, S. A. H., et al. 2003, *A&A*, 402, 87
- Ho, L. C., & Peng, C. Y. 2001, *ApJ*, 555, 650
- Hryniewicz, K., Czerny, B., Nikola juk, M., & Kuraszewicz, J. 2010, *MNRAS*, 404, 2028
- Hutchings, J. B., & Campbell, B. 1983, *Nature*, 303, 584
- Inoue, S., & Takahara, F. 1996, *ApJ*, 463, 555
- Ivezi ,  ., Menou, K., Knapp, G. R., et al. 2002, *AJ*, 124, 2364
- Jang, M., & Miller, H. R. 1997, *AJ*, 114, 565
- Jiang, D. R., Cao, X., & Hong, X. 1998, *ApJ*, 494, 139
- Jim nez-Bail n, E., Piconcelli, E., Guainazzi, M., et al. 2005, *A&A*, 435, 449
- Kaastra, J. S., & de Korte, P. A. J. 1988, *A&A*, 198, 16

- Kardashev, N. S. 1962, *Soviet Ast.*, 6, 317
- Kawaguchi, T., Shimura, T., & Mineshige, S. 2001, *ApJ*, 546, 966
- Kellermann, K. I., Sramek, R., Schmidt, M., Shaffer, D. B., & Green, R. 1989, *AJ*, 98, 1195
- Kirk, J. G., Rieger, F. M., & Mastichiadis, A. 1998, *A&A*, 333, 452
- Konigl, A. 1981, *ApJ*, 243, 700
- Kukula, M. J., Dunlop, J. S., Hughes, D. H., & Rawlings, S. 1998, *MNRAS*, 297, 366
- Laor, A., & Davis, S. W. 2011, *MNRAS*, 417, 681
- Lawson, A. J., & Turner, M. J. L. 1997, *MNRAS*, 288, 920
- Leipski, C., Falcke, H., Bennert, N., Hüttemeister, S. 2006, *A&A*, 455, 161
- Liu, B. F., Mineshige, S., & Shibata, K. 2002, *ApJ*, 572, L173
- Liu, H. T., Bai, J. M., Zhao, X. H., & Ma, L. 2008, *ApJ*, 677, 884
- Liu, Y., Jiang, D. R., & Gu, M. F. 2006, *ApJ*, 637, 669
- Malkan, M. A., & Sargent, W. L. W. 1982, *ApJ*, 254, 22
- McDowell, J. C., Canizares, C., Elvis, M., et al. 1995, *ApJ*, 450, 585
- McEnery, J. E., Moskalenko, I. V., & Ormes, J. F. 2004, *Cosmic Gamma-Ray Sources*, 304, 361
- Merloni, A., & Fabian, A. C. 2002, *MNRAS*, 332, 165
- Merloni, A., & Fabian, A. C. 2001, *MNRAS*, 328, 958
- Merloni, A., Heinz, S., & di Matteo, T. 2003, *MNRAS*, 345, 1057
- Miller, P., Rawlings, S., & Saunders, R. 1993, *MNRAS*, 263, 425
- Nandra, K., George, I. M., Mushotzky, R. F., Turner, T. J., & Yaqoob, T. 1997, *ApJ*, 488, L91
- Neugebauer, G., Oke, J. B., Becklin, E. E., & Matthews, K. 1979, *ApJ*, 230, 79
- Plotkin, R. M., Anderson, S. F., Brandt, W. N., et al. 2010, *ApJ*, 721, 562
- Popović, L. Č., Mediavilla, E. G., Bon, E., Stanić, N., & Kubičela, A. 2003, *ApJ*, 599, 185



- Rybicki, G. B., & Lightman, A. P. 1979, New York, Wiley-Interscience, 1979. 393 p.,
- Sakimoto, P. J., & Coroniti, F. V. 1981, *ApJ*, 247, 19
- Salvi, N. J., Page, M. J., Stevens, J. A., et al. 2002, *MNRAS*, 335, 177
- Schmidt, M., & Green, R. F. 1983, *ApJ*, 269, 352
- Schnopper, H. W., Delvaille, J. P., Epstein, A., et al. 1978, *ApJ*, 222, L91
- Shakura, N. I., & Sunyaev, R. A. 1973, *A&A*, 24, 337
- Shang, Z., Brotherton, M. S., Wills, B. J., et al. 2011, *ApJS*, 196, 2
- Shields, G. A. 1978, *Nature*, 272, 706
- Sikora, M., Begelman, M. C., & Rees, M. J. 1994, *ApJ*, 421, 153
- Sikora, M., Stawarz, L., & Lasota, J.-P. 2007, *ApJ*, 658, 815
- Strateva, I. V., Brandt, W. N., Schneider, D. P., Vanden Berk, D. G., & Vignali, C. 2005, *AJ*, 130, 387
- Sun, W.-H., & Malkan, M. A. 1989, *ApJ*, 346, 68
- Svensson, R., & Zdziarski, A. A. 1994, *ApJ*, 436, 599
- Taam, R. E., & Lin, D. N. C. 1984, *ApJ*, 287, 761
- Tavecchio, F., Maraschi, L., Pian, E., et al. 2001, *ApJ*, 554, 725
- Tavecchio, F., Maraschi, L., & Ghisellini, G. 1998, *ApJ*, 509, 608
- Ulvestad, J. S., Antonucci, R. R. J., & Barvainis, R. 2005, *ApJ*, 621, 123
- Unger, S. W., Lawrence, A., Wilson, A. S., Elvis, M., & Wright, A. E. 1987, *MNRAS*, 228, 521
- Wang, T.-G., Zhou, H.-Y., Wang, J.-X., Lu, Y.-J., & Lu, Y. 2006, *ApJ*, 645, 856
- White, R. L., Becker, R. H., Gregg, M. D., et al. 2000, *ApJS*, 126, 133
- Wilkes, B. J., & Elvis, M. 1987, *ApJ*, 323, 243
- Zdziarski, A. A., Lubiński, P., & Smith, D. A. 1999, *MNRAS*, 303, L11

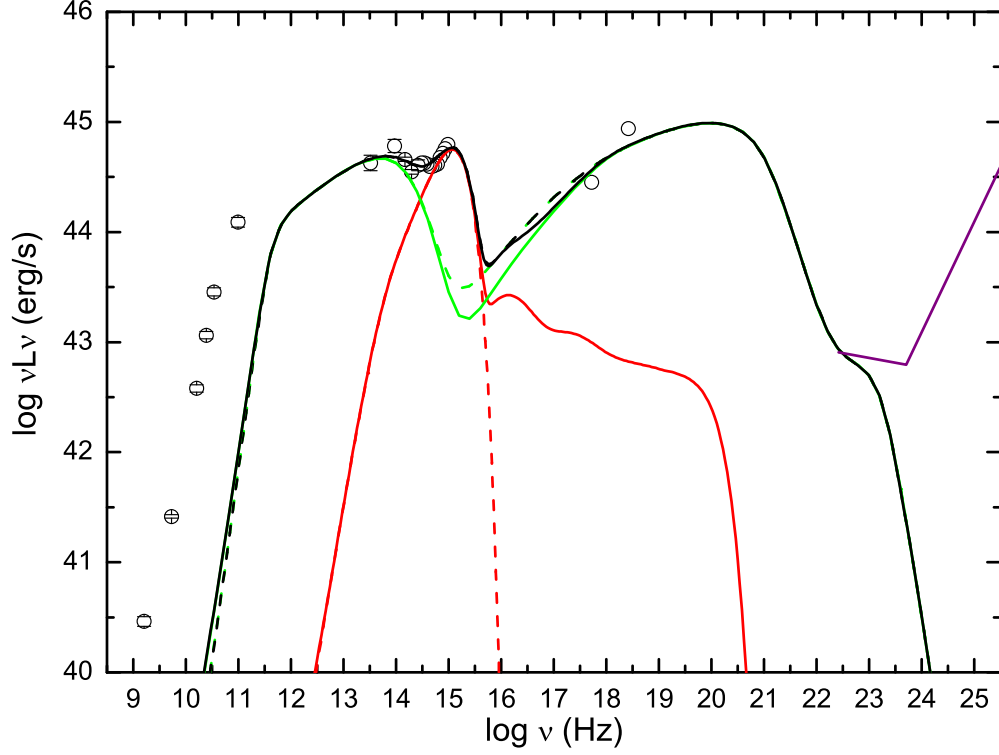


Fig. 1.— The quasi-simultaneous SED of III Zw 2 (see Table 2 for references of the data). The method of least squares is used to fit SED. The green solid line represents the emission from the jet, while the red solid line is for the disk/corona emission. The red dashed line represents the spectra from the bare accretion disk, while the green dashed line is for the emission from the jet in this case. The black line is the sum of the emission from the jet and the accretion disk/corona. The purple line represents the sensitivity of  $\gamma$ -ray detector *Fermi*/LAT (McEnery et al. 2004). The parameters model calculations see Table 1.

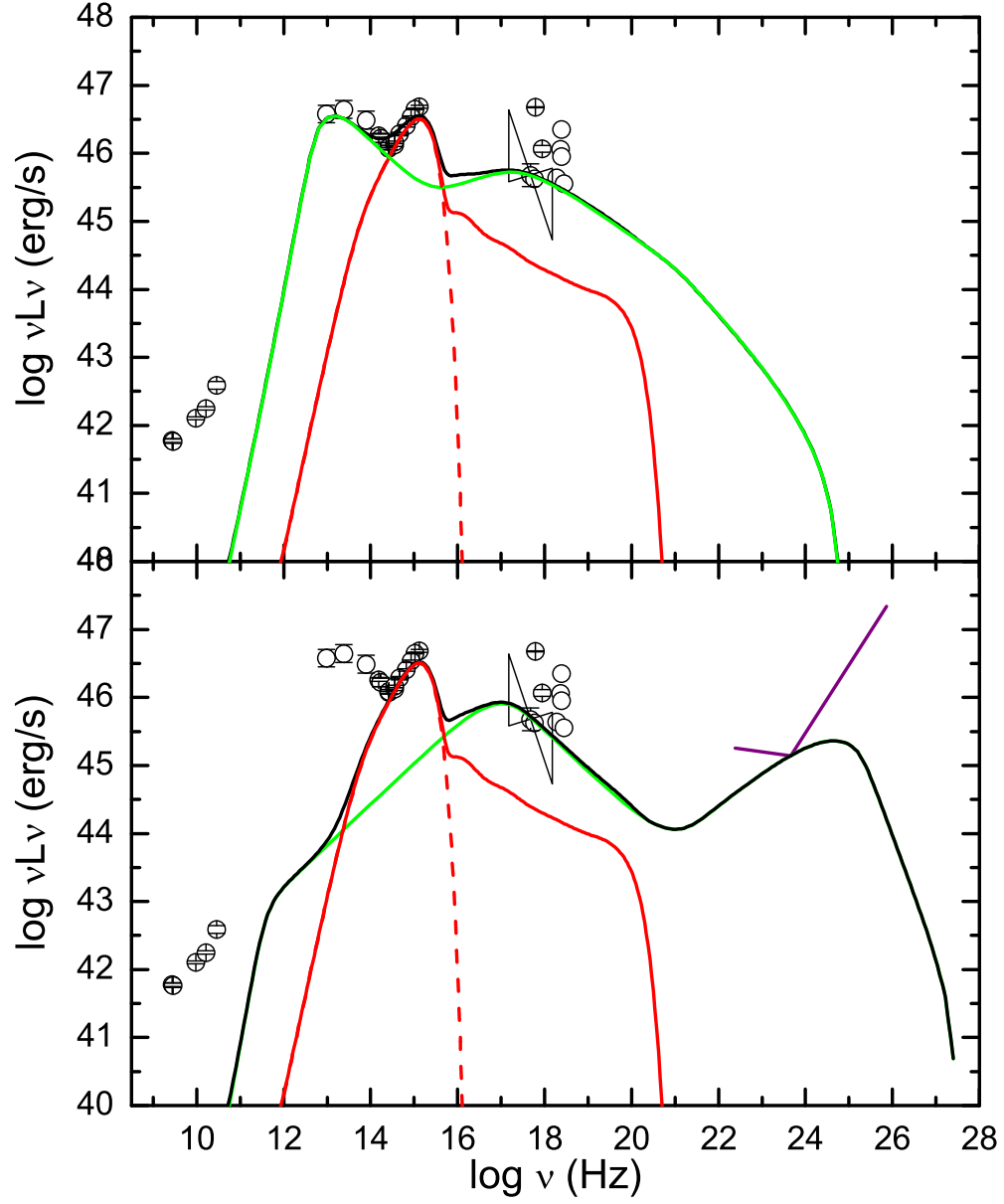


Fig. 2.— The same as Figure 1, but for the source of PG 1407+265. The method of least squares is used in fitting.

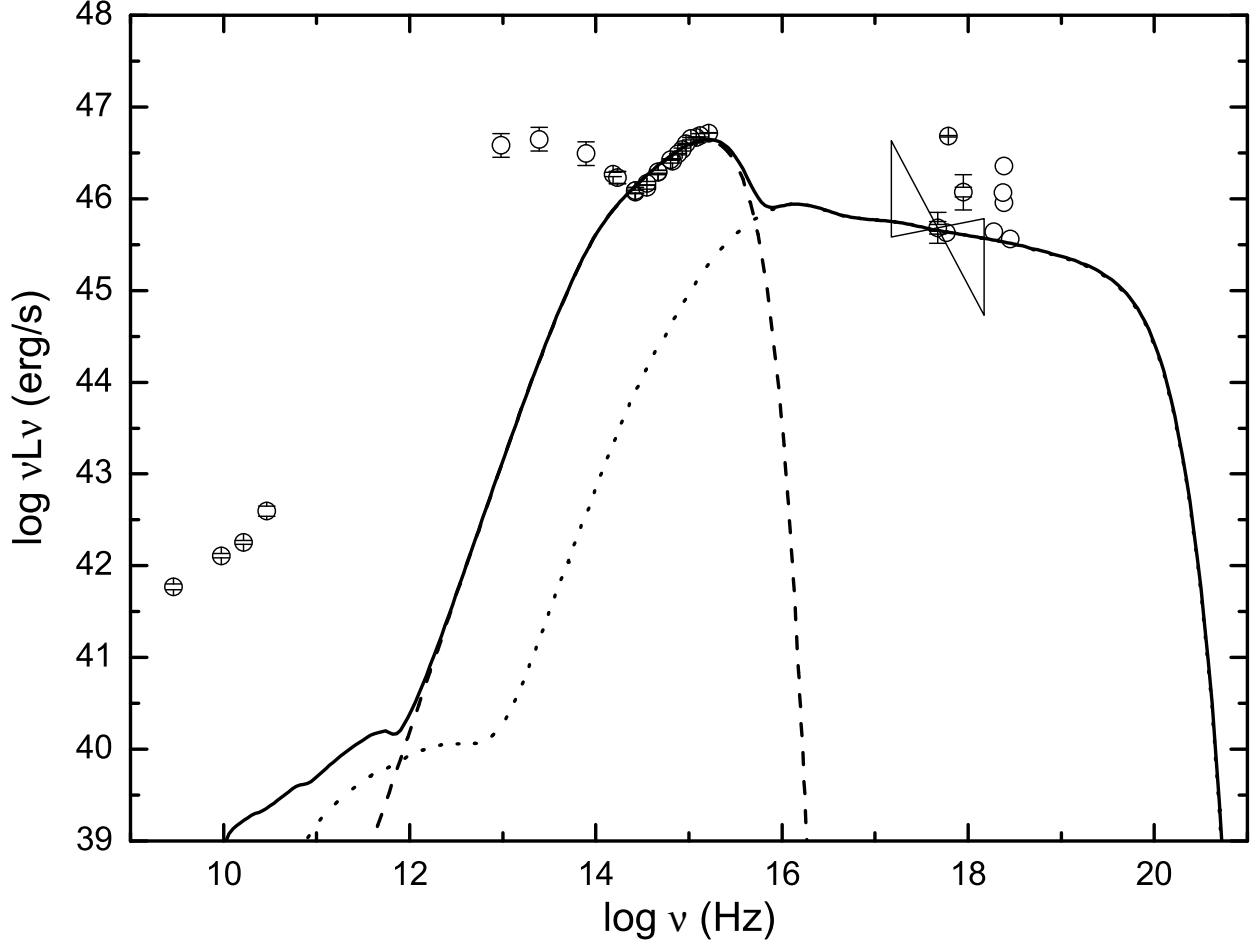


Fig. 3.— The same as Figure 2, but the SED is fitted with the accretion disk/corona model. The magnetic stress  $\tau_{r\varphi} = \alpha p_{\text{tot}}$  is used, and the best-fitted model parameters are:  $\dot{m} = 0.3$  and  $\alpha = 0.5$ . The solid line represents the spectra from the accretion disk/corona system. The dashed line represents the disk spectra, while the dotted line is for the spectra from the corona.

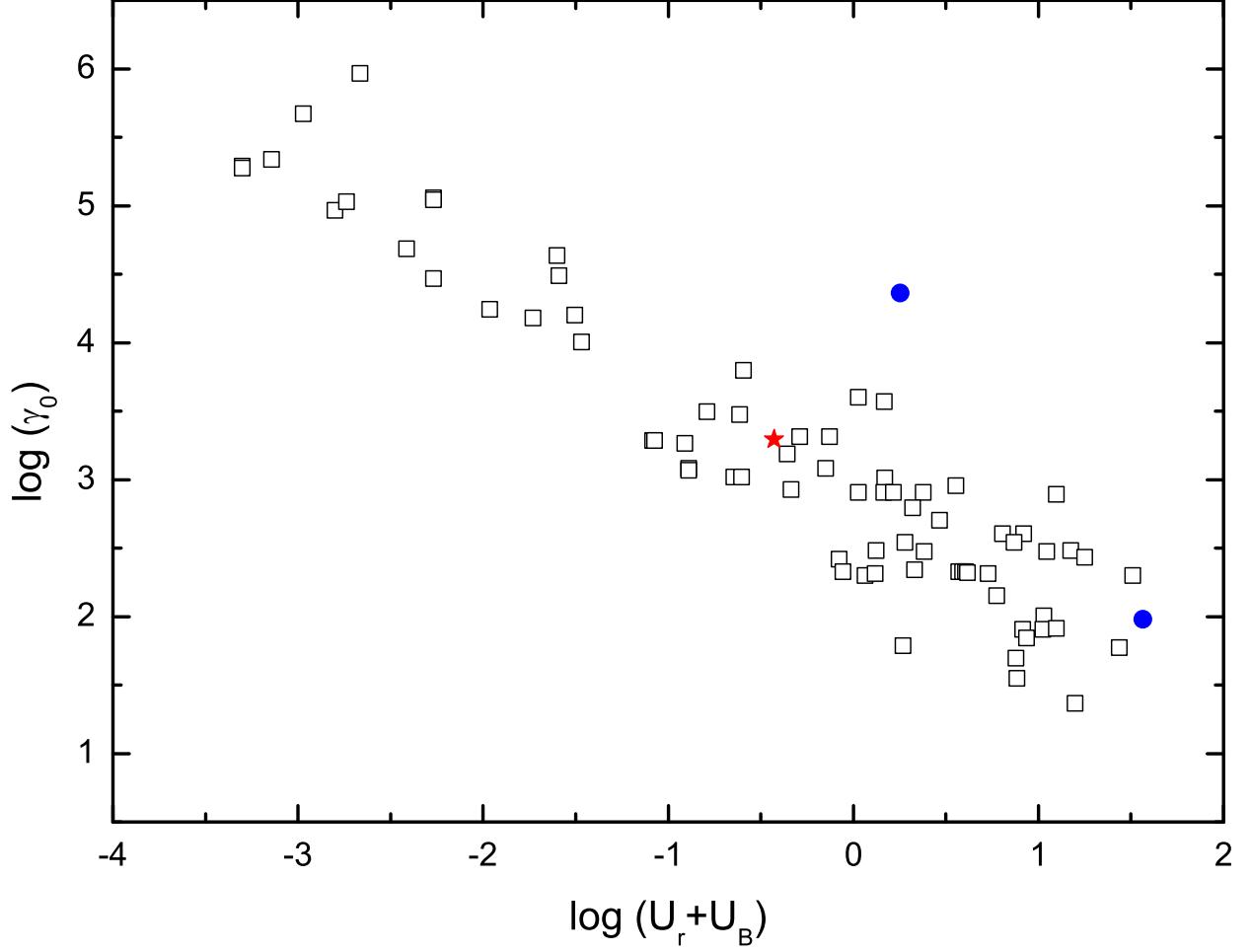


Fig. 4.— The blazar sequence:  $\gamma_0$  vs.  $U'_{\text{tot}}$ . The opened squares represent the blazars taken from Celotti & Ghisellini (2008). The red stars represent III Zw 2, while the blue dots indicate PG 1407+265. The dot with a higher  $\gamma_0$  corresponds to the case with the X-ray emission dominated by the synchrotron emission from the jet, while the lower one corresponds to the case of the X-ray emission emission dominated by the inverse Compton scattering in the jet.

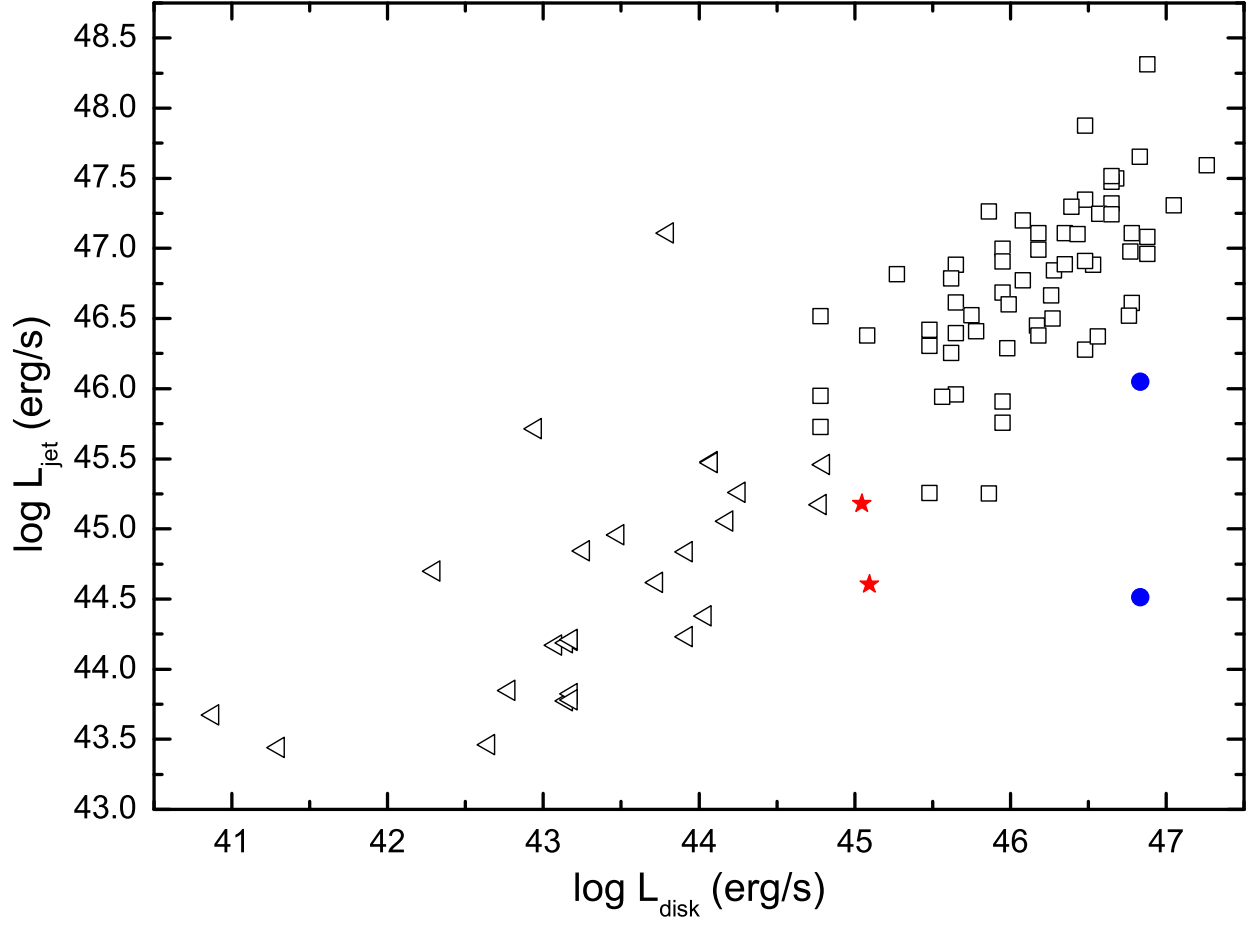


Fig. 5.— Jet power  $L_{\text{jet}}$  vs. disk luminosity  $L_{\text{disk}}$ . The black triangles/squares present the blazars, while the triangles are for the sources only with upper limits on the disk luminosity (see, Ghisellini et al. 2010). The red stars represent III Zw 2, while the blue dots are for PG 1407+265. The dot with lower jet power corresponds to the case of the X-ray emission dominated by the synchrotron emission from the jet, while the higher one is for case of the X-ray emission dominated by the inverse Compton scattering in the jet.

Table 1. Parameters of III Zw 2

Model	$B(\text{Gs})$	$N_0$	$p_1$	$p_2$	$\gamma_0$	$\gamma_{\min}$	$\dot{m}$	$\alpha$	$\tau_{r\varphi}$	$L_{\text{jet}}^\dagger$	$L_{\text{disk}}^\dagger$
1	2.08	$7.02 \times 10^5$	2.3	7.0	1963	20.0	$5.1 \times 10^{-3}$	...	...	1.51	1.12
2	2.08	$7.02 \times 10^5$	2.3	7.0	1963	58.1	$1.0 \times 10^{-2}$	0.2	$\alpha \sqrt{p_{\text{gas}} p_{\text{tot}}}$	0.40	1.25

Note. —  $^\dagger$   $L_{\text{jet}}$  and  $L_{\text{disk}}$  are in unit of  $10^{45}$  erg/s.  $B$  is the magnetic field,  $N_0$  the normalized number density,  $p_{1,2}$  the indexes of the broken power law electron energy distribution,  $\gamma_0$  the peak electron energy,  $\gamma_{\min}$  the minimum electron energies,  $\dot{m}$  the dimensionless accretion rate,  $\alpha$  the viscosity parameter. Model 1 indicates the dashed line in Figure 1. Model 2 is for the solid line in Figure 1.

Table 2. quasi-simultaneous SED data of III Zw 2

$\log \nu$	$\log f_\nu(\text{Jy})$	Observation Date	Ref.
9.166	$-1.000 \pm 0.043$	Jan. 1978	S78
9.689	$-0.569 \pm 0.016$	Jan. 1978	S78
10.169	$0.114 \pm 0.033$	Jan. 1978	S78
10.352	$0.415 \pm 0.033$	Jan. 1978	S78
10.497	$0.663 \pm 0.038$	Jan. 1978	S78
10.954	$0.839 \pm 0.044$	Jan. 1978	S78
13.480	$-1.150 \pm 0.070$	Jul. 1977	N79
13.934	$-1.450 \pm 0.060$	Jul. 1977	N79
14.134	$-1.770 \pm 0.020$	Jul. 1977	N79
14.260	$-2.010 \pm 0.020$	Jul. 1977	N79
14.380	$-2.070 \pm 0.050$	Jul. 1977	N79
14.450	-2.120	Jul. 1977	N79
14.500	-2.170	Jul. 1977	N79
14.550	-2.230	Jul. 1977	N79
14.600	-2.300	Jul. 1977	N79
14.650	-2.350	Jul. 1977	N79
14.700	-2.390	Jul. 1977	N79
14.750	-2.430	Jul. 1977	N79
14.800	-2.420	Jul. 1977	N79
14.850	-2.430	Jul. 1977	N79
14.900	-2.440	Jul. 1977	N79
14.950	-2.450	Jul. 1977	N79
17.680	-5.523	Aug. 1977	K88
18.379	-5.732	Aug. 1977	K88

Note. — The quasi-simultaneous spectra of III Zw 2 as plotted in Figure 1. The reference S78 refers to Schnopper et al. (1978), N79: Neugebauer et al. (1979), K88: Kaastra & de Korte (1988).



Table 3. SED data of PG 1407+265

$\log \nu$	$\log f_\nu(\text{Jy})$	Observation Date	Ref.
9.17	-2.06 $\pm$ 0.03	Sep. 1993	B96
9.69	-2.24 $\pm$ 0.02	Sep. 1993	B96
9.93	-2.33 $\pm$ 0.02	Sep. 1993	B96
10.17	-2.23 $\pm$ 0.06	Sep. 1993	B96
12.69	-0.77 $\pm$ 0.13	Jun. 1996	H03
13.10	-1.11 $\pm$ 0.13	Jun. 1996	H03
13.61	-1.77 $\pm$ 0.13	Jun. 1996	H03
13.90	-2.29 $\pm$ 0.02	Apr. 1988	E94, <i>NED</i>
13.95	-2.37 $\pm$ 0.06	Apr. 1988	E94, <i>NED</i>
13.95	-2.37 $\pm$ 0.07	Apr. 1988	E94, <i>NED</i>
14.13	-2.70 $\pm$ 0.03	Apr. 1988	E94, <i>NED</i>
14.13	-2.72 $\pm$ 0.02	Apr. 1988	E94, <i>NED</i>
14.13	-2.70 $\pm$ 0.03	Apr. 1988	E94, <i>NED</i>
14.83	-2.80 $\pm$ 0.02	May 1986	E94, <i>NED</i>
14.73	-2.73 $\pm$ 0.01	May 1986	E94, <i>NED</i>
14.64	-2.76 $\pm$ 0.02	May 1986	E94, <i>NED</i>
14.53	-2.78 $\pm$ 0.02	May 1986	E94, <i>NED</i>
14.38	-2.75 $\pm$ 0.02	May 1986	E94, <i>NED</i>
14.38	-2.74 $\pm$ 0.02	May 1986	E94, <i>NED</i>
14.26	-2.79 $\pm$ 0.02	Apr. 1988	E94, <i>NED</i>
14.26	-2.75 $\pm$ 0.02	Apr. 1988	E94, <i>NED</i>
17.38	-6.36 $\pm$ 0.17	...	<i>NED</i>
17.48	-6.51	...	<i>NED</i>
17.50	-5.47 $\pm$ 0.01	...	<i>NED</i>
17.66	-6.25 $\pm$ 0.05	...	<i>NED</i>
17.99	-7.00	...	<i>NED</i>
18.08	-6.67	...	<i>NED</i>
18.10	-6.80	...	<i>NED</i>
18.10	-6.40	...	<i>NED</i>
18.16	-7.26	...	<i>NED</i>

Note. — SED data of PG 1407+265 as plotted in Figures 2 and 3. The reference B96 refers to Barvainis et al. (1996), H03: Haas et al. (2003), E94: Elvis et al. (1994), *NED*: <http://ned.ipac.caltech.edu/>.

Table 4. X-ray spectra of PG 1407+265

Observation Date	flux <sup>†</sup>	Photon index	$f_{2-10\text{keV}}^{\ddagger}$	Telescope	Ref.
Jan. 17, 1981	$f_{1\text{keV}} = 0.44_{-0.05}^{+0.17} \mu\text{Jy}$	$\Gamma = 2.2_{-0.4}^{+1.7}$	1.27	EINSTEIN	W87
Jun. 19-20, 1987	$f_{2-10\text{keV}} = 0.12 \times 10^{-11} \text{ erg/cm}^2/\text{s}$	...	1.2	GINGA	L97
Jan. 19, 1992	$f_{1\text{keV}} = 1.0_{-0.04}^{+0.04} \mu\text{Jy}$	$\Gamma = 2.61_{-0.05}^{+0.05}$	1.62	ROSAT	M95
Jul. 02, 1993	$f_{2-10\text{keV}} = 1.38_{-0.04}^{+0.04} \times 10^{-12} \text{ erg/cm}^2/\text{s}$	$\Gamma = 2.05_{-0.05}^{+0.05}$	1.38	ASCA	G00
Jan. 23, 2001	$L_{2-10\text{keV}} = 8.85 \times 10^{45} \text{ erg/s}$	$\Gamma = 2.32_{-0.02}^{+0.02}$	1.33	XMM-Newton	G06
Dec. 22, 2001	$f_{2-10\text{keV}} = 0.8 \times 10^{-12} \text{ erg/cm}^2/\text{s}$	$\Gamma = 2.24_{-0.02}^{+0.01}$	0.8	XMM-Newton	F05

Note. — X-ray spectra of PG 1407+265. <sup>†</sup> flux presented in references. <sup>‡</sup> 2-10 keV integral flux (in unit of  $10^{-12} \text{ erg/cm}^2/\text{s}$ ) calculated from the flux<sup>†</sup> and the  $\Gamma$ . The reference W87 refers to Wilkes & Elvis (1987), L97: Lawson & Turner (1997), M95: McDowell et al. (1995), G00: George et al. (2000), G06: Gallo (2006), F05: Fang et al. (2005).

Table 5. Parameters of PG 1407+265

Model	$B(\text{Gs})$	$N_0$	$R^{\dagger}$	$p_1$	$p_2$	$\gamma_0$	$\gamma_{\text{min}}$	$\dot{m}$	$\alpha$	$\tau_{\text{r}\varphi}$	$L_{\text{jet}}^{\ddagger}$	$L_{\text{disk}}^{\ddagger}$
1	29.4	$1.7 \times 10^5$	4.2	1.8	4.2	95	13.5	0.08	1.0	$\alpha \sqrt{p_{\text{gas}} p_{\text{tot}}}$	11.3	68.1
2	5.0	$1.8 \times 10^3$	4.2	1.8	4.2	23148	4.6	0.08	1.0	$\alpha \sqrt{p_{\text{gas}} p_{\text{tot}}}$	0.33	68.1
3	...	...	...	...	...	...	...	0.3	0.5	$\alpha p_{\text{tot}}$	...	144

Note. — <sup>†</sup>  $R$  is the radius of emission region in unit of  $10^{15} \text{ cm}$ . <sup>‡</sup>  $L_{\text{jet}}$  and  $L_{\text{disk}}$  are in unit of  $10^{45} \text{ erg/s}$ . The model parameters have the same meanings as those in Table 1. Model 1 corresponds to the upper panel of Figure 2. Model 2 is for the lower panel of Figure 2. Model 3 corresponds to the result in Figure 3.